Author Accepted Manuscript

Accepted by *Scripta Materialia*, 7 March 2019

Phase separation process preventing thermal embrittlement of a Zr-Cu-Fe-Al bulk metallic glass

D. V. Louzguine-Luzgin[1,2*], J. Jiang[3], A. I. Bazlov[4], V.S. Zolotorevzky[4], H. Mao[5,6], Yu. P. Ivanov[7] and A.L. Greer[7,1]

[1] *WPI Advanced Institute for Materials Research, Tohoku University, Sendai, 980-8577, Japan*

[2] *Mathematics for Advanced Materials-OIL, National Institute of Advanced Industrial Science and Technology (AIST), Sendai 980-8577, Japan*

[3] *Graduate School of Engineering, Tohoku University, Sendai, 980-8577, Japan*

[4] *National University of Science and Technology "MISiS", Moscow, 119049, Russia*

[5] *KTH Royal Institute of Technology, Department of Materials Science and Engineering, 10044 Stockholm, Sweden*

[6] *Thermo-Calc Software AB, Råsundavägen 18, 16967 Solna, Sweden*

[7] *Department of Materials Science & Metallurgy, University of Cambridge, Cambridge, CB3 0FS, UK*

Abstract

The structural changes and mechanical properties of $Zr_{63}Cu_{22}Fe_5Al_{10}$ bulk metallic glass (BMG), and a $Zr_{63}Cu_{27}Al_{10}$ glass made for comparison, were studied on annealing below the crystallization temperature. The phase composition of the samples was studied by conventional X-ray diffractometry and high-resolution transmission electron microscopy including the atomic-scale elemental mapping. The samples were mechanically tested in compression. The $Zr_{63}Cu_{22}Fe_5Al_{10}$ bulk metallic glass shows high strength and good deformability at room temperature both in the as-cast state and after prolonged structural relaxation below the crystallization temperature. The reasons for such behavior are discussed in the present work.

---

* Corresponding author, e-mail: dml@wpi-aimr.tohoku.ac.jp, Tel: +081(22)217-5957, Fax: +081(22)217-5957

Keywords: bulk metallic glass; mechanical properties; relaxation; phase separation; transmission electron microscopy.

Metallic glasses (MGs) [1,2], particularly bulk metallic glasses (BMGs) [3,4] produced by casting [5] or other methods [6], attract significant attention because of their high strength, high hardness, good wear resistance [7] and large elastic deformation [8,9]. Although most BMGs lack plasticity even in the as-cast state, there are several examples of monolithic BMGs with significant plasticity [10,11].

Typically, annealing of BMGs in the temperature range starting from about 200 K below T_g causes structural relaxation [12] and embrittlement [13]. For example, significant embrittlement of the $Zr_{52.5}Cu_{17.9}Ni_{14.6}Al_{10}Ti_5$ BMG was found in the temperature range 373–573 K [14]. Reduction of the excess volume upon annealing can drastically embrittle metallic glasses by shrinking the plastic zone at crack tips [15]. Hypoeutectic Fe-B glasses are reported to be sensitive to thermal embrittlement when B begins to saturate the corresponding atomic cages in the disordered iron network [16]. It was also shown that Cu-Zr-Al alloys are not sensitive to thermal embrittlement [17] owing to the formation of ordered nanoscale areas and deformation-induced crystallization in the annealed glass. Similar ordered zones were found in annealed Cu-Hf-Ti-Pd glassy alloys [18].

Here we report on a Zr-based BMG which is not prone to thermal embrittlement under low-temperature annealing, yet remaining fully amorphous.

Ingots of $Zr_{63}Cu_{27}Al_{10}$ and $Zr_{63}Cu_{22}Fe_5Al_{10}$ (at.%) alloys were prepared by arc-melting high-purity (>99.9 mass.%) elements in a Ti-gettered Ar atmosphere. Rectangular rods of 2×2 mm section and several centimeters long were formed by injection-casting into a copper mold.

The density of the BMG samples was measured by the Archimedean method in liquid tetrabromoethane. The phase composition of the samples was checked by conventional X-ray diffractometry (XRD) with monochromatic CuKα radiation, while thermal stability was tested by differential scanning calorimetry at a heating rate of 0.67 K s^{-1}.

Rectangular samples 4 mm long and 2×2 mm cross section with parallel polished ends cut from the as-cast and annealed samples were tested mechanically in compression using an Instron 5581 universal testing machine. Vickers microhardness (H_V) was measured at 2.94 N load with 15 s indentation time, while each quoted value is an average of at least 10 independent measurements. The

95% confidence interval was determined using the student's distribution (t). The value of t is a function of the desired significance level $\alpha = 0.05$ at N–1 degrees of freedom.

Transmission electron microscopy (TEM) observation of the samples was carried out using JEOL JEM2010F and FEI Tecnai Osiris microscopes with field-emission gun TEM/STEM facilities operated at 200 keV, the latter one equipped with Super-X windowless EDX detector. The samples for TEM were prepared by Ar ion polishing with a liquid-nitrogen cooling system.

Thermodynamic calculations of the phase diagrams were performed using the Thermo-Calc software dataset taken from Ref. [19].

The as-cast samples were found to be fully glassy (Fig. 1a, insert). The relaxation and crystallization behavior was studied by DSC (Fig. 1) and found to be very similar for both alloys. For example, T_g values of 664 and 665 K were obtained, respectively, for $Zr_{63}Cu_{27}Al_{10}$ and $Zr_{63}Cu_{22}Fe_5Al_{10}$. As in the case of other Zr-Cu-system metallic glasses [20,21] the structural relaxation process starts at a reduced temperature T_r about 200 K below T_g.

Fig. 1b shows the mechanical properties of both alloys at room temperature. The Zr-Cu-Al alloy was quite brittle even in the as-cast state, while the Zr-Cu-Fe-Al alloy shows room-temperature plasticity even after annealing at a high temperature close to T_g. No clear difference in the deformation behavior is found. The magnitude of each stress drop as a function of strain is shown in Fig. 2c. The arrow shows a transition from a deformation process proceeding by multiple bands to shear localization in a dominant shear band [22]. As it is a stochastic process [23] the formation of a dominant shear band takes place at different strain values but a transition threshold at about 25 MPa of the stress drop magnitude is seen in all samples. The $Zr_{63}Cu_{27}Al_{10}$ BMG remains brittle after annealing.

The sample annealed at 623 K showed almost identical deformation behavior to the as-cast one (Fig. 1b,c). SEM observation showed (Fig. 2) that, in case of the annealed samples, the minor shear bands are localized in the vicinity of a dominant shear band which led to fracture, while in the as-cast sample the shear bands are more widely distributed within the lateral surface of the broken sample.

The density and length changes of the studied alloys upon annealing nearly 25 K below T_g are shown in Table 1. At a relatively large sample length of about 30 mm the precision in length-change

measurements is better than that in density changes. Both samples show densification after annealing, though the densification process in both density and length changes is slower in the case of the quaternary alloy. No detectable length changes were found after annealing at 573 K. The Vickers microhardness of the $Zr_{63}Cu_{22}Fe_5Al_{10}$ glassy alloy changes from H_V 502±8 in the as-cast state to H_V 489±4 after annealing at 573 K for 1 h and H_V 489±5 after annealing at 623 K for 1 h. A small decrease in the Vickers microhardness is correlated with the value of yield stress, decreasing from 1560 MPa in the as-cast state to 1540 MPa after annealing at 573 K for 1 h and to 1500 MPa after annealing at 623 K for 1 h (Fig. 1b).

The structure of $Zr_{63}Cu_{22}Fe_5Al_{10}$ was also studied by transmission electron microscopy in the annealed state (623 K, 1 h). The as-cast structure looks homogeneous (Fig. 1), while some inhomogeneities with a characteristic lengthscale of about 10 nm are clearly observed in the large-scale HRTEM image (Fig. 2e) obtained after annealing at 625 K for 1 h, though the structure remains clearly glassy without any traces of crystallinity (Fig. 2f).

Fig. 3a-d shows the atomic elemental maps of the Zr-Cu-Fe-Al sample annealed for 1 h at 623 K produced using EDX technique. An inhomogeneous antiphase spatial distribution of Zr and Cu elements is clearly seen. As marked with the circles, local maxima of Fe content also correspond to local minima of Cu content which is expected from the slightly positive mixing enthalpy for this atomic pair.

A statistical analysis (Fig. 3e-h) indicates that all elements are distributed inhomogeneously (a bimodal distribution is observed) while Al atoms are rather randomly distributed in the map as its content follows a single-mode Gaussian distribution.

Separation into Zr- and Cu-rich areas (Fig. 3) is unusual taking into account the negative mixing enthalpy in this system of about –17 kJ mol^{-1} at equiatomic composition and –12 kJ mol^{-1} at 3:1 Zr to Cu ratio in liquid state [24], and no other local minima in this system except for the central one. However, a non-monotonic behavior of the mixing enthalpy was found in a Zr-(Cu+Al) section of ternary Zr-Cu-Al system [19]. In order to explain the observed separation, thermodynamic calculations were made and indicated the existence of the metastable miscibility gap in Zr-Cu-rich area of Zr-Cu-Al system as shown Fig. 4. Even though there are no atomic pairs with a positive mixing enthalpy in the Zr-Cu-Al system,

phase separation still can take place in the case of sub-regular solutions. The calculated Gibbs energy of formation at 273, 373 and 473 K for the metastable liquid of the Cu-Zr binary system indicates a slight curvature change at low temperatures on the Zr-rich side, which indicates a tendency for phase separation into CuZr- and Zr-rich phases. This is not the case in Al-Zr or Fe-Zr binary alloys. Phase separation was also observed earlier in a Zr-Cu-Fe-Al alloy on annealing in the supercooled liquid region and at that time was believed to be a result of Cu-Fe interaction with positive mixing enthalpy [19]. It is likely that Fe having a positive mixing enthalpy with Cu further promotes the low-temperature phase separation process. The onset of phase separation was also observed in Zr-Cu-Fe-Al alloy on mechanical cyclic loading before crystallization [25]. The tendency for Cu and Fe to separate is also seen on the atomic distribution maps in Fig. 3.

Zr-Cu-Fe-Al bulk metallic glasses [26,27] do not contain pre-existing nuclei, and crystallize by nucleation and growth type reaction. The embrittlement of metallic glasses upon annealing is associated with a reduction in the excess "free" volume [28] or reduction in the Poisson's ratio [29,30], thus degrading its capacity for plastic flow. Although the majority of metallic glasses embrittle on heating during structural relaxation, here it is found that the $Zr_{63}Cu_{22}Fe_5Al_{10}$ alloy is insensitive to thermal embrittlement in the relaxed state. Moreover, one can observe a slight decrease in hardness and yield strength even though the samples are reduced in length and volume on relaxation. The observed increase in density of about 0.2 % is again quite typical for the relaxed Zr-based bulk metallic glasses [31].

It is proposed that such behavior in the Zr-Cu-Fe-Al alloy is connected with the nanoscale phase separation within the glassy phase which is confirmed by the elemental mapping in TEM (see Figs. 2 and 3) and suggested by thermodynamic modeling (Fig. 4). Aluminum is rather homogeneously distributed while other elements, especially Zr and Cu, exhibit clearly an inhomogeneous spatial distribution (Fig. 3). The distribution of Fe is also inhomogeneous. The reason for homogeneous distribution of Al is unclear, though Al was also found to be insensitive to variation in Zr and Cu content on the boundary between the metallic glass and surface oxide [32]. On the other hand the addition of Al was found to be the reason for the non-monotonic behavior of the mixing enthalpy found in a Zr-(Cu+Al) section of ternary Zr-Cu-Al system [19].

Phase separation is observed in many metallic glasses. In many cases, it is caused by positive mixing enthalpy between a couple of alloying elements [33]. Phase separation was found to improve plasticity of the Zr-Cu-Co-Al [34] and Cu-Zr-Al-Co [35] bulk metallic glasses in the as-cast state (nanoscale phase separation) and can be a possible source of good plasticity of Zr-Cu-Ni-Al BMGs [36]. Also, in view of the current results, it is not clear whether phase separation in the Zr-Cu-Co-Al and Cu-Zr-Al-Co alloys was caused by positive mixing enthalpy in the Co-Cu atomic pair. Also, inhomogeneous binodal-type phase separation was observed in the $Cu_{43}Zr_{43}Al_7Ag_7$ [37] and $Cu_{36}Zr_{48}Al_8Ag_8$ bulk glassy alloys on heating [38]. The phase separation in the as-cast $Cu_{43}Zr_{43}Al_7Ag_7$ bulk metallic glass was related to its good plasticity [37], yet the latter BMG did not show plasticity after annealing [39].

Phase separation was observed in Ni-Nb-Y glasses on cooling [40] and by severe plastic deformation [41] owing to repulsive Nb–Y atomic interaction, but these alloys did not show significant plasticity. Pd-Ni-P [42] and Pd-Ni-Si-P glassy alloys [43] also showed some chemical inhomogeneity and, while the later alloys are deformable in compression, the former alloys are usually brittle and become ductile at high Ni content [44].

Rather surprisingly, structural inhomogeneity was observed in the nearly eutectic $Fe_{90}Zr_{10}$ metallic glass [45] and in the $Zr_{50}Cu_{50}$ one [46] on annealing below the crystallization temperature. Phase separation is not expected in these systems with strongly negative mixing enthalpy between the constituent elements. What is the thermodynamic stimulus of such a phase transformation? For example, the enthalpy [47] and Gibbs free energy [48] curves in the Zr-Cu system as a function of composition have a monotonic character. By analogy with our recent work on Ti-based alloy [49] one can suggest that chemical inhomogeneity in these alloys is caused by local chemical ordering within the incubation period as a trigger for nanocrystallization of a glassy phase or highly supercooled liquid.

However, phase separation into Y-rich and Zr-rich amorphous phases found in the $Cu_{46}Zr_{47-x}Y_xAl_7$ alloys above 15 at.% Y content caused extreme brittleness of the samples while the single-phase amorphous alloys at $x = 2$ and 5 were ductile in compression [50]. Phase separation in a $Fe_{40}Ni_{40}B_{20}$ alloy did not prevent its embrittlement [51]. Although the $Cu_{59}Zr_{41}$ metallic glass shows phase separation on annealing at 710 K (at about 50 nm of the characteristic lengthscale) its strain to fracture values drop drastically after some seconds of annealing.

Interaction of shear bands with structural inhomogeneities in the form of crystalline nanoparticles precipitated from the glassy matrix was systematically analyzed in Ref. [52]. At a particle size below 35 nm the absorption mechanism was suggested to be predominant, that is the shear bands propagate though such a structure basically in the same way as through the monolithic glassy phase. However, as the propagation speed of the shear bands was not determined it is possible that such a composite structure leads to a decrease in the shear-band propagation speed. Also, no clear difference in the morphology of shear bands can be seen from Fig. 2 between the as-cast and the annealed sample. Only, in the annealed sample the shear steps on the surface made by shear bands are more concentrated in the area close to the dominant shear band formed at the later deformation stage.

Thus, one could suggest that a number of factors: the lengthscale of the separated area as well as the elastic and plastic characteristics of the separated regions determine the plasticity of the samples. The variation of the composition causes variation in density and properties: the local shear modulus and Poisson ratio are also different in these areas of different composition. It is known that Cu-rich BMGs are in general harder and less plastic than Zr-rich, and phase-separated areas should have different mechanical properties [9]. The elastoplastic crack-tip instability of relaxed glasses was suggested to cause thermal embrittlement of metallic glasses [53]. Following that, one can suggest that the absence of embrittlement and even softening observed in the alloy is connected with the phase separation lengthscale of ~10 nm. This lengthscale exactly corresponds to the suggested thickness of the shear bands [54], though the affected region by the excess volume diffusion can be larger [55,56]. Larger phase separation lengthscales, such as ~50 nm found in the $Cu_{46}Zr_{47-x}Y_xAl_7$ alloys, are harmful from the viewpoint of high plasticity [50].

In conclusion, the studied $Zr_{63}Cu_{22}Fe_5Al_{10}$ metallic glass, even in the relaxed state, exhibits nearly as high plasticity as in the as-cast state. Also, no hardening but even mechanical softening is observed after annealing even though the samples showed a reduction in size and volume typical for fully relaxed Zr-based alloys. The reason for such behavior is connected with nanoscale phase separation at about 10 nm lengthscale within the glassy phase which is comparable in size to the thickness of shear bands. Formation of Cu- and Zr-rich areas on annealing at low temperature is also suggested by thermodynamic

calculations while Al is homogeneously distributed. Fe is also placed in antiphase with Cu and likely further promotes phase separation.

Acknowledgements

This work was supported by the World Premier International Research Center Initiative (WPI), MEXT, Japan and by the Ministry of Education and Science of the Russian Federation in the framework of the Program to Increase the Competitiveness of NUST "MISiS" (K2-2014-013 and K2-2017-089). ALG and YPI acknowledge support from the European Research Council under the European Union's Horizon 2020 research and innovation programme (grant ERC-2015-AdG-695487: Extend Glass).

References

[1] W. Klement, R.H. Willens, P. Duwez, Nature 187 (1960) 869–870.

[2] A.L. Greer, Nat. Mater. 14 (2015) 542–546.

[3] A. Inoue, Acta Mater. 48 (2000) 279–306.

[4] W.L. Johnson, MRS Bull. 24 (1999) 42–56.

[5] F. Haag, S. Geisel, G. Kurtuldu, J.F. Löffler, Acta Mater. 151 (2018) 416–423.

[6] M. Petrzhik, V. Molokanov, E. Levashov, J. Alloys Comp. 707 (2017) 68–72.

[7] D.V. Louzguine-Luzgin, M. Ito, S.V. Ketov, A.S. Trifonov, J. Jiang, C.L. Chen, K. Nakajima, Intermetall. 93 (2018) 312–317.

[8] C. Suryanarayana, A. Inoue, *Bulk Metallic Glasses*, CRC Press, Boca Raton, FL, 2011.

[9] D.V. Louzguine-Luzgin, in A. Zhukov (ed.) *Novel Functional Magnetic Materials, Fundamentals and Applications*, Vol. 231, Springer Series in Materials Science, Springer, Switzerland (2016), pp. 397–440.

[10] Y. Yokoyama, K. Fujita, A.R. Yavari, A. Inoue, Philos. Mag. Lett. 89 (2009) 322–334.

[11] B. Sarac, Yu.P. Ivanov, A. Chuvilin, T. Schöberl, M. Stoica, Z.L. Zhang, J. Eckert, Nat. Comm. 9 (2018) 1333.

[12] T.J. Lei, L.R. DaCosta, M. Liu, W.H. Wang, Y.H. Sun, A.L. Greer, M. Atzmon, Acta Mater. 164 (2019) 165–170.

[13] P. Murali, U. Ramamurty, Acta Mater. 53 (2005) 1467–1478.

[14] W. Li, Y. Gao, H. Bei, Sci. Reports 5 (2015) 14786.

[15] T.W. Wu, F. Spaepen, Philos. Mag. B 61 (1990) 739–750.

[16] A.R. Yavari, Mater. Sci. Eng. 98 (1988) 491–493.

[17] W. Guo, R. Yamada, J. Saida, Mater. Sci. Eng. A 699 (2017) 81–87.

[18] D.V. Louzguine-Luzgin, I. Seki, T. Yamamoto, H. Kawaji, C. Suryanarayana, A. Inoue, Intermetall. 23 (2012) 177–181.

[19] C.Y. Zhou, C.P. Guo, C.G. Li, Z.M. Du, J. Non-Cryst. Solids 461 (2017) 47–60.

[20] D.V. Louzguine-Luzgin, I. Seki, T. Wada, A. Inoue, Metall. Mater. Trans. A 43 (2012) 2642–2648.

[21] D.V. Louzguine-Luzgin, A.R. Yavari, M. Fukuhara, K. Ota, G.Q. Xie, G. Vaughan, A. Inoue, J. Alloys Comp. 431 (2007) 136–140.

[22] D.V. Louzguine-Luzgin, V.Yu. Zadorozhnyy, N. Chen, S.V. Ketov, J. Non-Cryst. Solids 396–397 (2014) 20–24.

[23] D.V. Louzguine-Luzgin, D.M. Packwood, G. Xie, A.Yu. Churyumov, J. Alloys Comp. 561 (2013) 241–246.

[24] H.M. Hsiao, S.M. Liang, R.S. Fetzer, Y.V. Yen, Calphad 55 (2016) 77–87.

[25] A.Yu. Churyumov, A.I. Bazlov, V.Yu. Zadorozhnyy, A.N. Solonin, A. Caron, D.V. Louzguine-Luzgin, Mater. Sci. Eng. A 550 (2012) 358–362.

[26] K.F. Jin, J.F. Loffler, Appl. Phys. Lett. 86 (2005) 241909.

[27] Q.S. Zhang, W. Zhang, D.V. Louzguine-Luzgin, A. Inoue, Mater. Sci. Forum, 654–656 (2010) 1042–1045.

[28] T.W. Wu, F. Spaepen, Philos. Mag. B 61 (1990) 739–750.

[29] J.J. Lewandowski, W.H. Wang, A.L. Greer, Philos. Mag. Lett. 85 (2005) 77–87.

[30] G.R. Garrett, M.D. Demetriou, M.E. Launey, W.L. Johnson, PNAS 113 (2016) 10257–10262.

[31] O. Haruyama, K. Yoshikawa, Y. Yamazaki, Y. Yokoyama, T. Egami, Mater. Trans. 56 (2015) 648–654.

[32] D.V. Louzguine-Luzgin, C.L. Chen, L.Y. Lin, Z.C. Wang, S.V. Ketov, M.J. Miyama, A.S. Trifonov, A.V. Lubenchenko, Y. Ikuhara, Acta Mater. 97 (2015) 282–290.

[33] D.H. Kim, W.T. Kim, E.S. Park, N. Mattern, J. Eckert, Prog. Mater. Sci. 58 (2013) 1103–1172.

[34] J.M. Park, J.H. Han, N. Mattern, D.H. Kim, J. Eckert, Metall. Mater. Trans. A. 43 (2012) 2598–2603.

[35] W. Zhou, Y.M. Tao, L. Liu, L.T. Kong, J.F. Li, Y.H. Zhou, Mater. Trans. 54 (2013) 286–290.

[36] Y.H. Liu, G. Wang, R.J. Wang, D.Q. Zhao, M.X. Pan, W.H. Wang, Science 315 (2007) 1385–1388.

[37] J.C. Oh, T. Ohkubo, Y.C. Kim, E. Fleury, K. Hono, Scripta Mater. 53 (2005) 165–169..

[38] D.V. Louzguine-Luzgin, T. Wada, H. Kato, J.H. Perepezko, A. Inoue, Intermetall. 18 (2010) 1235–1239.

[39] J. Gu, L.X. Zhang, Y.H. Wang, S. Ni, S.-F. Guo, M. Song, Trans. Nonferr. Met. Soc. China 26 (2016) 1620−1628.

[40] N. Mattern, U. Kühn, A. Gebert, T. Gemming, M. Zinkevich, H. Wendrock, Scripta Mater. 53 (2005) 271–274.

[41] A.A. Mazilkin, G.E. Abrosimova, S.G. Protasova, B.B. Straumal, G. Schutz, S.V. Dobatkin, A.S. Bakai, J. Mater. Sci. 46 (2011) 4336–4340.

[42] S. Lan, Y. Ren, X.Y. Wei, B. Wang, E.P. Gilbert, T. Shibayama, S. Watanabe, M. Ohnuma, X.-L. Wang, Nat. Comm. 8 (2017) 14679.

[43] D.V. Louzguine-Luzgin, N. Chen, V.Yu. Zadorozhnyy, I. Seki, A. Inoue, Intermetall. 33 (2013) 67–72.

[44] D.V. Louzguine-Luzgin, Y. Zeng, A.D.H. Setyawan, N. Nishiyama, H. Kato, J. Saida, A. Inoue, J. Mater. Res. 22 (2007) 1087–1092.

[45] G.E. Abrosimova, A.S. Aronin, J. Surf. Invest. 9 (2015) 887–893.

[46] R. Schulz, K. Samwer, W.L. Johnson, J. Non-Cryst. Solids 61 (1984) 997–1002.

[47] M.A. Turchanin, Powder Metall. Met. Ceram. 39 (1997) 253–263.

[48] A.I. Zaitsev, N.E. Zaitseva, Yu.P. Alekseeva, E.M. Kuril'chenko, S.F. Dunaev, Inorg. Mater. 39 (2003) 816–825, transl. from Neorg. Materialy 39 (2003) 954–963.

[49] Z. Wang, C.L. Chen, S.V. Ketov, K. Akagi, A.A. Tsarkov, Y. Ikuhara, D.V. Louzguine-Luzgin, Mater. Design 156 (2018) 504–513.

[50] E.S. Park, D.H. Kim, Acta Mater. 54 (2006) 2597–2604.

[51] J. Piller, P. Haasen, Acta Metall. Mater. 30 (1982) 1–8.

[52] A.M. Glezer, N.A. Shurygin, S.G. Zaichenko, I.E. Permyakova, Russ. Metall. (Metally) 2013 (2013) 235–244.

[53] C.H. Rycroft, E. Bouchbinder, Phys. Rev. Lett. 109 (2012) 194301.

[54] Y. Zhang, A.L. Greer, Appl. Phys. Lett. 89 (2006) 071907.

[55] J. Pan, Q. Chen, L. Liu, Y. Li, Acta Mater. 59 (2011) 5146–5158.

[56] S.V. Ketov, H.K. Nguyen, A.S. Trifonov, K. Nakajima, D.V. Louzguine-Luzgin, J. Alloys Comp. 687 (2016) 221–226.

Figure captions

Fig. 1. (a) DSC traces of both alloys. The insert shows an HRTEM image together with the SAED pattern of the $Zr_{63}Cu_{22}Fe_5Al_{10}$ BMG in the as-cast state. (b) Engineering compressive stress-strain curves of the $Zr_{63}Cu_{27}Al_{10}$ (as-cast) and $Zr_{63}Cu_{22}Fe_5Al_{10}$ (as-cast and heat-treated, as indicated) glassy alloys. (c) The magnitude of stress drops in the stress-strain curves after yielding as a result of each serration.

Fig. 2. SEM images of the lateral surfaces of the as-cast sample (a,b) and the sample annealed at 623 K (c,d) after fracture. (a,c) are obtained near the fracture surface and (b,d) at a distance from that. HRTEM images of the Zr-Cu-Fe-Al sample annealed for 1 h at 623 K (e) at low magnification together with a SAED pattern, insert and (f) at high magnification.

Fig. 3. (a-d) The elemental maps for Zr, Cu, Fe and Al, respectively, plotted for the Zr-Cu-Fe-Al sample annealed for 1 h at 623 K. (a-d) Frequency distribution of the concentration of the constituent elements Zr, Cu, Fe and Al, respectively, obtained from the data shown in Fig. 4. Zr, Cu and Fe show bimodal distributions while Al rather follows a single-mode Gaussian distribution. Some variation from the exact chemical composition is observed owing to calibration difficulties of the EDX machine.

Fig. 4. (a) Calculated metastable phase separation region of a highly supercooled liquid in the Al-Cu-Zr ternary system at different isotherms (T = 200, 300, 400 °C, i.e. 473, 573 and 673 K). There is no

miscibility gap above ~430 °C. (b) Calculated Gibbs free energy of formation at 273, 373 and 473 K for the metastable liquid of the Cu-Zr binary system. Thermodynamic data are taken from [19].

TABLES

Table 1. The density (ρ) values of the studied alloys in the as-cast state (ac) and after annealing (an) as well as the corresponding percentage changes (Δ%) of the samples annealed at 640 K for 1 and 2 h, as indicated. The measurement error for the density values is $\pm$0.003 g cm^{-3}.

Alloy (1 h)	ρ_{ac}, g cm^{-3}	ρ_{an}^{1h}, g cm^{-3} (Δ%)	ρ_{an}^{2h}, g cm^{-3} (Δ%)
$Zr_{63}Cu_{27}Al_{10}$	6.664	6.683 (+0.29 %)	6.688 (+0.36 %)
$Zr_{63}Cu_{22}Fe_5Al_{10}$	6.635	6.643 (+0.12 %)	6.651 (+0.24 %)

Table 2. The length (L) values of the studied alloys in the as-cast state (ac) and after annealing (an) as well as the corresponding percentage changes (Δ%) and approximate volume change (ΔV%) of the samples annealed at 640 K for 1 and 2 h. The measurement error for the length changes is $\pm$0.001 mm.

Alloy (1 h)	L_{ac}, mm	L_{an}^{1h}, mm (Δ%)	~ΔV^{1h} %	L_{an}^{2h}, mm (Δ%)	~ΔV^{2h} %
$Zr_{63}Cu_{27}Al_{10}$	30.271	30.246 (–0.08%)	–0.25 %	30.243 (–0.09%)	–0.28 %
$Zr_{63}Cu_{22}Fe_5Al_{10}$	30.005	29.986 (–0.06%)	–0.19 %	29.984 (–0.07%)	-–0.21 %

FIGURES

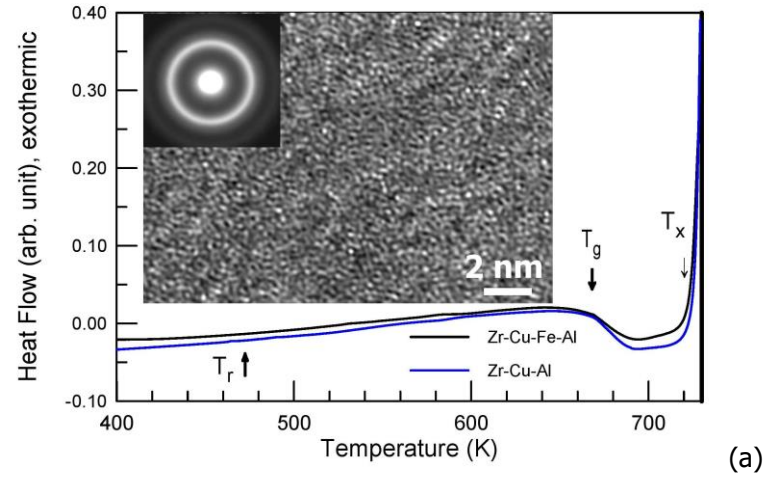

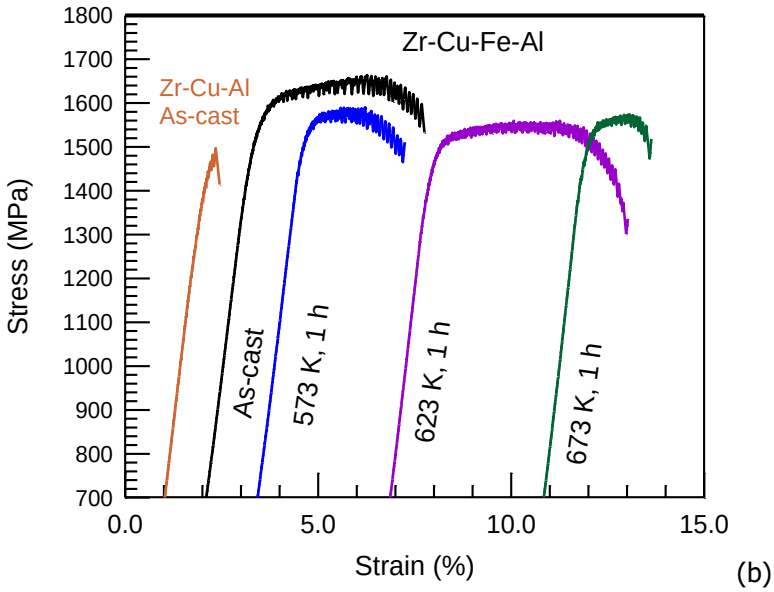

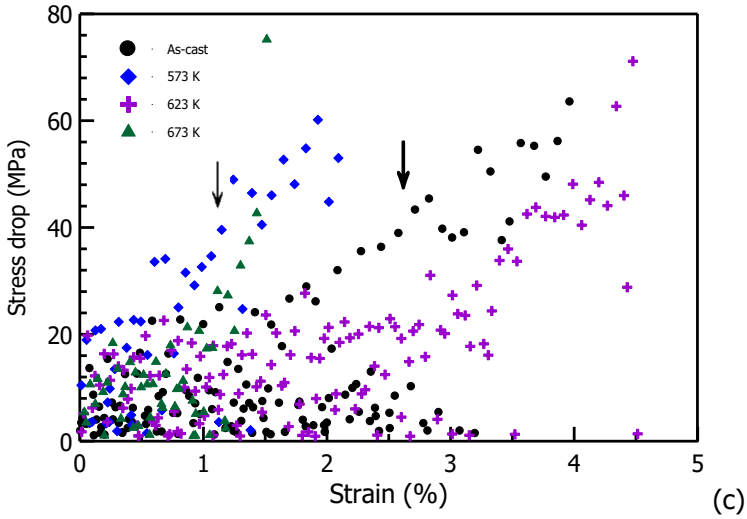

Fig. 1. (a) DSC traces of both alloys. The insert shows an HRTEM image together with the SAED pattern of the $Zr_{63}Cu_{22}Fe_5Al_{10}$ BMG in the as-cast state. (b) Engineering compressive stress-strain curves

of the $Zr_{63}Cu_{27}Al_{10}$ (as-cast) and $Zr_{63}Cu_{22}Fe_5Al_{10}$ (as-cast and heat-treated, as indicated) glassy alloys. (c) The magnitude of stress drops in the stress-strain curves after yielding as a result of each serration.

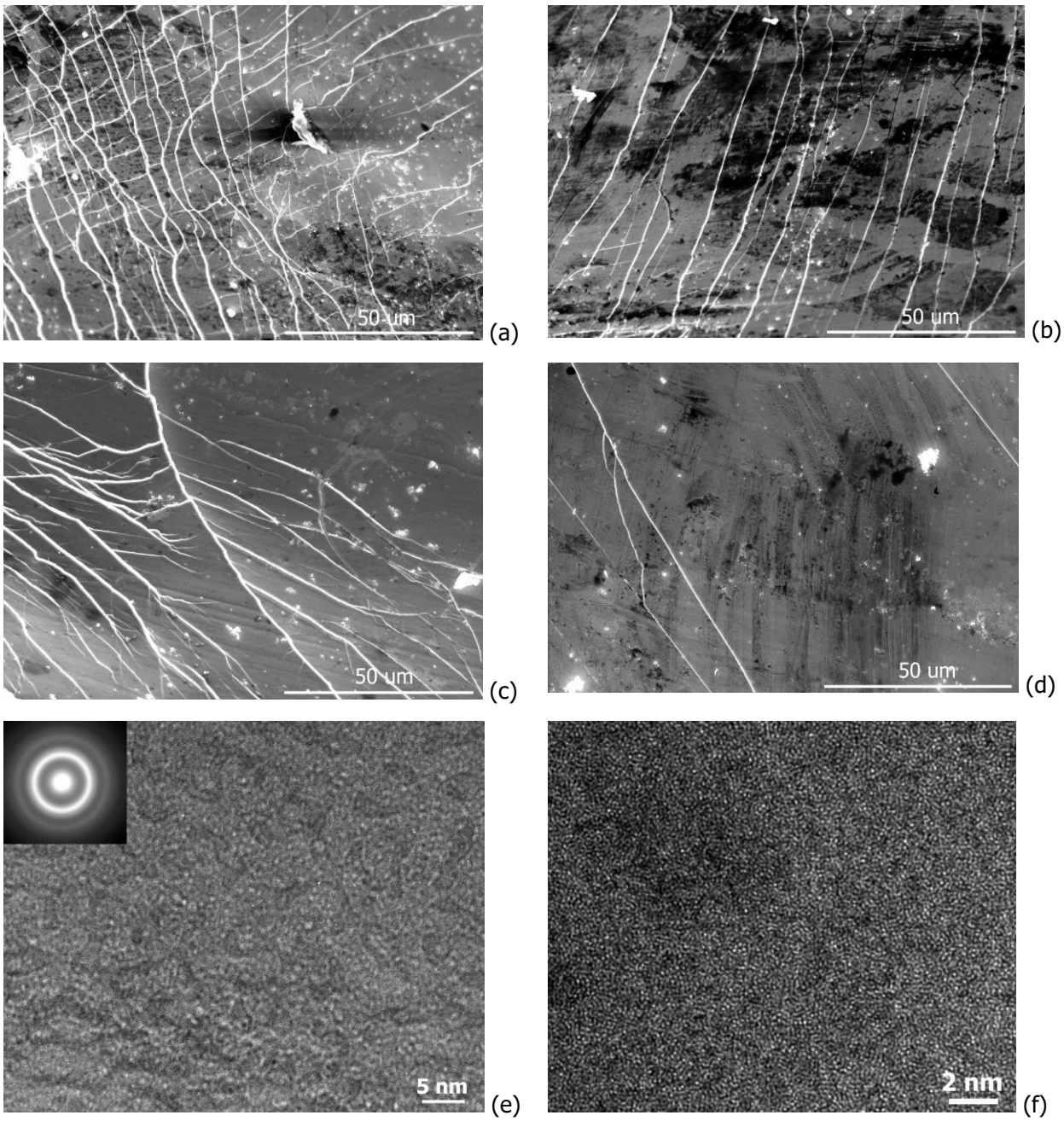

Fig. 2. SEM images of the lateral surfaces of the as-cast sample (a,b) and the sample annealed at 623 K (c,d) after fracture. (a,c) are obtained near the fracture surface and (b,d) at a distance from that. HRTEM images of the Zr-Cu-Fe-Al sample annealed for 1 h at 623 K (e) at low magnification together with a SAED pattern, insert and (f) at high magnification.

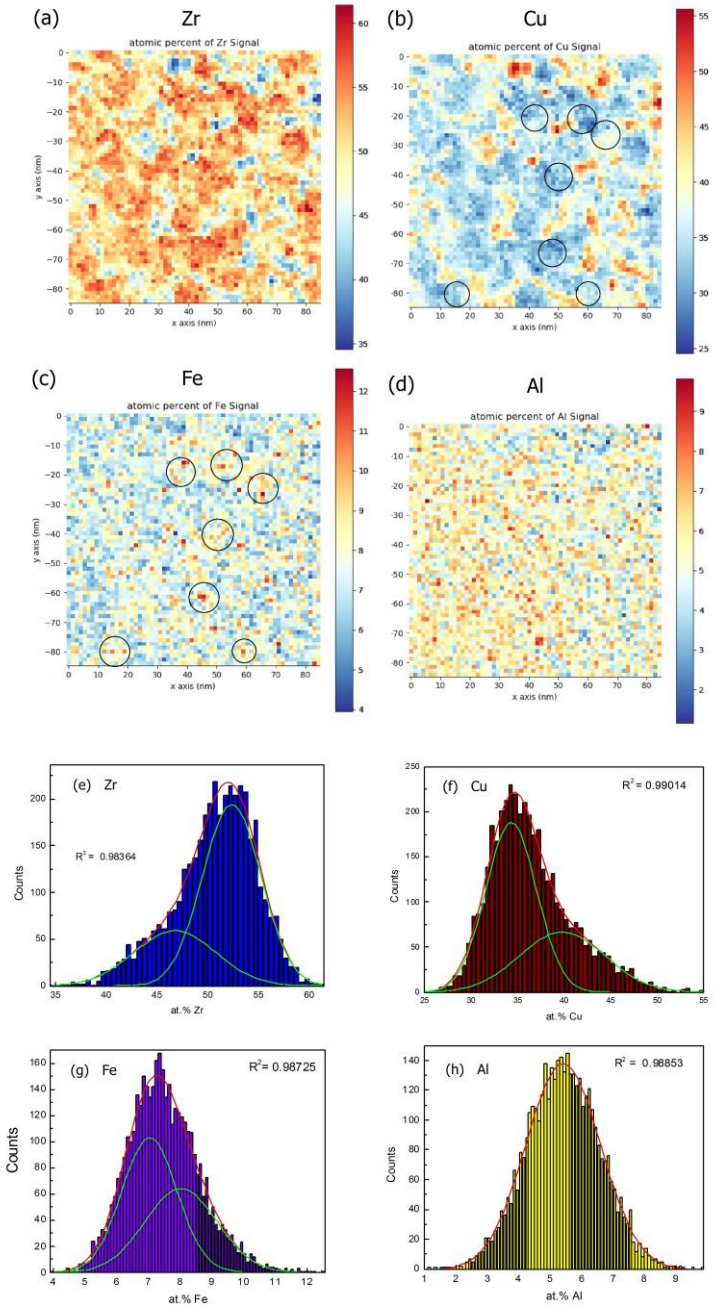

Fig. 3. (a-d) The elemental maps for Zr, Cu, Fe and Al, respectively, plotted for the Zr-Cu-Fe-Al sample annealed for 1 h at 623 K. (e-h) Frequency distribution of the concentration of the constituent elements Zr, Cu, Fe and Al, respectively, obtained from the data shown in (a-d). Zr, Cu and Fe show bimodal distributions while Al rather follows a single-mode Gaussian distribution. Some variation from the exact chemical composition is observed owing to calibration difficulties of the EDX machine.

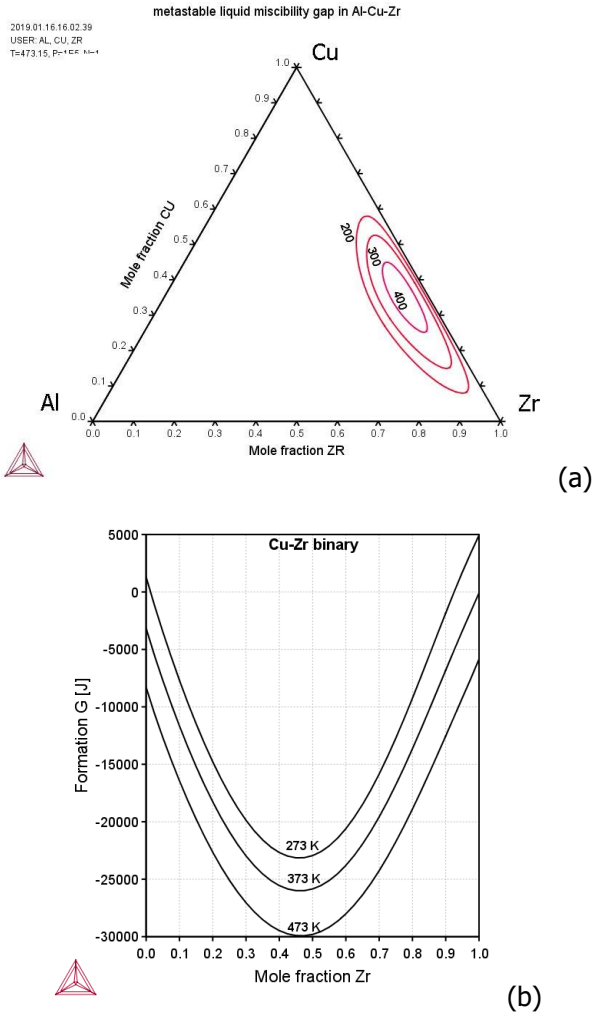

Fig. 4. (a) Calculated metastable phase separation region of a highly supercooled liquid in the Al-Cu-Zr ternary system at different isotherms (T = 200, 300, 400 °C, i.e. 473, 573 and 673 K). There is no miscibility gap above ~430 °C. (b) Calculated Gibbs free energy of formation at 273, 373 and 473 K for the metastable liquid of the Cu-Zr binary system. Thermodynamic data are taken from [19].